Nat. Hazards Earth Syst. Sci. Discuss., doi:10.5194/nhess-2017-49, 2017
Manuscript under review for journal Nat. Hazards Earth Syst. Sci.
Discussion started: 9 February 2017

Natural Hazards and Earth System Sciences Discussions

Using street view imagery for 3D survey of rock slope failures

Jérémie Voumard[1], Antonio Abellan[1,2], Pierrick Nicolet[1,3], Marie-Aurélie Chanut[4], Marc-Henri Derron[1], Michel Jaboyedoff[1]

[1] Risk analysis group, Institute of Earth Sciences, FGSE, University of Lausanne, Switzerland
[2] Scott Polar Research Institute, Department of Geography, University of Cambridge, United Kingdom
[3] Geohazard and Earth Observation team, Geological Survey of Norway (NGU), Norway
[4] Groupe Risque Rocheux et Mouvements de Sols (RRMS), Cerema Centre-Est, France

Correspondence to: Jérémie Voumard (jeremie.voumard@unil.ch)

Abstract. We discuss here the challenges and limitations on surveying rock slope failures using 3D reconstruction from images acquired from Street View Imagery (SVI) and processed with modern photogrammetric workflows. We show how the "back in time" function can be used for a 3D reconstruction of two or more image sets from the same site but at different instants of time, allowing for rock slope surveying. Three sites in the French alps were selected: (a) a cliff beside a road where a protective wall collapsed consisting on two images sets (60 and 50 images on each set) captured on a six years timeframe; (b) a large-scale active landslide located on a slope at 250 m from the road, using seven images sets (50 to 80 images per set) from five different time periods with three images sets for one period; (c) a cliff over a tunnel which has collapsed, using three images sets on a six years time-frame. The analysis includes the use of different commercially available Structure for Motion (SfM) programs and comparison between the so-extracted photogrammetric point clouds and a LiDAR derived mesh used as a ground truth. As a result, both landslide deformation together with estimation of fallen volumes were clearly identified in the point clouds. Results are site and software-dependent, as a function of the image set and number of images, with model accuracies ranging between 0.1 and 3.1 m in the best and worst scenario, respectively. Despite some clear limitations and challenges, this manuscript demonstrates that this original approach might allow obtaining preliminary 3D models of an area without on-field images. Furthermore, the pre-failure topography can be obtained for sites where it would not be available otherwise.

Keyword

Street view imagery, Structure from Motion, photogrammetry, 3D point cloud, natural hazard, landslide, rockfall.

1 Introduction

3D remote sensing techniques are becoming widely used for geohazard investigations due to their ability to represent the geometry of natural hazards (mass movements, lava flows, debris flows, etc.) and its evolution over time by comparing 3D point clouds acquired at different time steps. For example, 3D remote sensing techniques are helping to better quantify key

aspects of rock slope evolution, including the accurate quantification of rockfall rates and the deformation of rock slopes before failure using both LiDAR (Rosser et al., 2005; Oppikofer et al, 2009; Royan et al., 2013; Kromer et al., 2015; Fey and Wichmann., 2016) and photogrammetrically derived point clouds (Walstra et al., 2007; Lucieer et al., 2013, Stumpf et al., 2015; Fernandes et al., 2016; Guerin et al., 2016; Ruggles et al., 2016).

Airborne and terrestrial laser scanner (ALS and TLS, respectively) are commonly used techniques to obtain 3D digital terrain models. Despite their very high accuracy and resolution, these technologies are expensive and demanding from a logistic point of view (Abellan et al., 2014). Another way to obtain point clouds without these inconveniences is photogrammetry, in particular the Structure from Motion (SfM) combined with multiview-stereo (MVS) that allow generating reasonably good 3D point clouds using end-user digital cameras (Westoby et al., 2012; Carrivick et al., 2016).

Whereas most of the studies in SfM literature utilise pictures that were directly captured on-site, the potential of using internet-retrieved pictures has been discussed before (e.g. Snavely et al., 2008). One of the large sources of pictures on-line is the Street View Imagery (SVI) services, which offer 360 degrees panoramas from many roads, streets and other places around the world (Anguelov et al, 2013). It allows to remotely observe areas at a very reduced cost and without physically accessing them. SVI is thus an interesting visual information source, with applications in navigation, tourism, building texturing, image localization, point clouds georegistration and motion-from-structure-from-motion (Zamir et al. 2010; Anguelov et al, 2010; Klingner et al, 2013; Wang, 2013; Lichtenauer et al., 2015).

The aim of present work is to ascertain whether 3D models be derived from SVI using photogrammetric workflows can be used to detect geomorphic changes on rock slopes.

1.1 Street View Imagery

The most common SVI service is the well-known Google Street View (GSV) (Google Street View, 2017) that is available from Google Maps (Google Maps, 2017) or Google Earth Pro (Google Earth Pro, 2013). We used both GSV as SVI service in this study. Alternatives include Streetside by Microsoft (Streetside, 2017) and other national services like Tencent Maps in China (Tencent Maps, 2017). SVI was firstly deployed in urban areas to offer a virtual navigation into the streets. More recently, non-urban zones can also be accessed, and will be used for the analysis of rock slope failures in this manuscript.

Firstly used in May 2007 for capturing pictures in streets of the main cities in USA, GSV has been deployed worldwide over the forthcoming years, including also rural areas. GSV images are collected with a panoramic camera system mounted on different types of vehicles (e.g. a car, train, bike, snowmobile, etc.) or carried into a backpack (Anguelov et al, 2010) (Figure 1).

The GSV first generation camera system was composed of eight wide-angle lenses and it is currently composed of fifteen CMOS sensors 5Mpx each (Anguelov et al, 2010). The fifteen raw images, which are not publicly available, are processed by Google to make a panorama view containing an a priori unknown image deformation. A GSV panorama is normally taken at an interval of around ten meters along a linear infrastructure (road, train, path).

Nat. Hazards Earth Syst. Sci. Discuss., doi:10.5194/nhess-2017-49, 2017
Manuscript under review for journal Nat. Hazards Earth Syst. Sci.
Discussion started: 9 February 2017

Natural Hazards and Earth System Sciences Discussions

GSV proposes a back-in-time function on a certain number of locations since April 2014. Historical GSV images are available from 2007 for selected areas only. The number of available image sets varies a lot because it depends on the number of acquisitions made by Google. While many locations have only one image set, some places have several sets. This function is especially useful for natural hazards because it is possible to compare pre- and post-events images.

The GSV process can be explained in four steps (Anguelov et al, 2010; Google Street View, 2017): (1) Pictures acquisition in the field; (2) Image alignment: preliminary coordinates are given for each picture, extracted from sensors on the Google car that measure GNNS coordinates, speed and azimuth of the car, helping to precisely reconstruct the vehicle path. Pictures can also be tilted and realigned as needed; (3) Creation of 360° panoramas by stitching overlapping pictures. Google applies a series of processing algorithms to each picture to attenuate delimitations between each picture and to obtain smooth pictures transitions; (4) Panoramas draping on 3D models: the three LiDAR mounted on the Google car help to build 3D models of the scenes. 360° panoramas are draped on those 3D models to give a panorama view close to the reality. Each picture of the panorama has its own internal deformation, and the application of the processing chain described above makes inconstant deformation in the 360° panorama; in addition, the end-user does not have any information or control on it.

1.2 SfM-MVS

Structure for Motion (SfM) with Multi-View Stereo (MVS) dense reconstruction is a low-cost photogrammetric method to obtain a 3D point cloud of terrain using a series of overlapping images (Luhmann et al., 2014). The prerequisites are that: (1) the studied object is photographed from different points of view, and (2) each element of the object must be captured from a minimum of two pictures assuming that the lens deformation parameters are known in advance (Snavely 2008; Lucieer et al. 2013). If these parameters are not known beforehand, three pictures is the minimum requirement (Westoby 2012), about six pictures is preferred. The particularity of SfM-MVS is that prior knowledge of both intrinsic camera parameters (principal point, principal distance and lens distortion) and extrinsic camera parameters (orientation and position of the camera centre (Luhmann et al., 2014)) is not needed.

The workflow of SfM-MVS normally includes the following steps: (1) Feature detection and matching (Lowe, 1999); (2) Bundle adjustment (Snavely et al., 2006; Favalli et al., 2011; Turner et al., 2012; Lucieer et al., 2013); (3) Dense 3D point cloud generation (Furukawa et al., 2010; Furukawa & Ponce, 2010; James & Robson, 2012); and (4) Surface reconstruction and visualization (James & Robson, 2012).

2. Study areas and available data

We selected three study areas in France to generate point clouds from GSV images. This country was chosen because GSV cover the majority of the roads and because the timeline function works in most of the areas covered by GSV, meaning that several periods of acquisition are available. Moreover, landslide events occur regularly on French alpine roads. The aerial view of the three areas is shown in Figure 2A and examples of corresponding GSV images in Figure 2B and 2C.

The first case study ("Basse corniche" site) is a 20 m high cliff beside a main road in Roquebrune – Cap Martin connecting the town of Menton to the Principality of Monaco, in South-Eastern France. A wall built to consolidate the cliff collapsed after an extreme rainfall event in January 2014, blocking the road (Nice-Matin, 2014). Two 3D models were built with 60 GSV images taken in 2008 before the wall collapse, and 50 GSV images taken in 2014 after the event.

The second case studies is Séchilienne landslide, located 15 km South East of Grenoble (Isère department, France). The active area is threatening the departmental road RD 1091 connecting the towns of Grenoble and Briançon as well as a set of ski resorts such as L'Alpe d'Huez and Les Deux Alpes to the plain. This landslide is about 800 m long by 500 m high and it has been active during more than thirty years (Le Roux et al. 2009; Durville et al. 2011; Dubois et al. 2014). The shortest distance between the landslide foot and the former road was 250 m. A new road, located higher in the opposite slope, has been opened since July 2016. Different SfM-MVS processing from GSV images were tested using from 50 up to 80 GSV images, at five different times from April 2010 to June 2015.

The third case study is located in "Arly gorges", between Ugine and Megève on the path Alberville – Chamonix-Mont-Blanc. A rockfall of about 8'000 m^3 affected the road at the entry of a tunnel on January 2014 (France 3, 2014). Three sets of images ranging from 60 to 110 GSV images were processed in order to obtain three 3D models of the road, the tunnel entry and the cliff above the tunnel.

We used two image sets from for the first study site, height images sets for the second study site and four image sets for the third study site, with dates ranging from May 2008 up to December 2016, as described in table 1.

3. Methodology

First step to make SfM-MVS with SVI is to get images from a SVI service. GSV has been used in this study (Figure 1). Given that original images of the Google cameras are not available, the only way to get images from GSV is to manually extract them from the GSV panoramas. We took print screens of GSV panoramas of the studied areas at each acquisition step (about ten meters). We took several images from the same point of view with different pan and tilt angles (Figure 1C) when the studied object was too close to the road. In such cases, it was impossible to have the entire area in one image because the image is not wide enough to capture the entire studied area (for example a 10 m high cliff along road). When the studied area was far away from the road, we took print screens of zoomed sections of the panorama.

To perform temporal comparisons on each site, images were taken at the different dates proposed by GSV. We used the SfM-MVS programs VisualSFM (Wu 2011) and Agisoft PhotoScan (Agisoft 2015) for dense point cloud reconstruction and CloudCompare (Girardeau-Montaut 2011) for point cloud visualization and comparison. Comparison between two point clouds was made using point-to-mesh strategy. A mesh of one point cloud (whether the point cloud with the oldest images for the site 1 or the LiDAR scans for the sites 2 and 3) is compared with the other point cloud to obtain the shortest distance of each point of the point cloud to the mesh in absolute values.

Beside the images taken from print screens as described above, we also obtained GSV images from Google Earth Pro on sites 2 and 3 with the "save image" function. Unfortunately, there is no timeline function in this program and it is only possible to save Google Earth Pro images from the last picture acquisition.

It is important to mention here that a series of issues are expected when attempting to use SVI for 3D model reconstruction with SfM-MVS. Indeed, GSV images are constructed as 360° panoramas from a series of pictures, so the internal deformation of the original image is not fully retained on the panoramas. In other words, the deformation of a cropped section of the panorama will be a main function not only of the internal deformation of the camera and lens but to the panorama reconstruction process; This circumstance will significantly influence the bundle adjustment process and so to the 3D reconstruction.

In addition, GoPro Hero4+ images from a moving vehicle on the road were taken by the authors on site 2, as well a series of images captured using a GoPro Hero5 Black camera standing on site 3. Six LiDAR scans were also taken on site 3. This information was used for quality assessment purposes.

4. Results and discussion

Different results are obtained as a function on the software used for SfM-MVS processing. VisualSFM gave the best results with print screens from GSV while Agisoft PhotoScan could not align any GSV images from Google Maps print screens despite adding a series of control points measured with Google Earth Pro. However, Agisoft PhotosScan provided better results with images from Google Earth Pro than VisualSFM.

4.1 Site 1 – "Basse corniche" site

It was possible on "Basse Corniche" site to estimate the fallen volume by scaling and comparing the 2008 and 2010 point clouds. VisualSFM software could align the images and make 3D models before and after the wall collapse. It was possible to roughly scale the scene with the road width measured on Google Earth Pro and on the French geoportal (Géoportail, 2016). After aligning the two 3D point clouds, meshes were built to compute the collapsed volume (Figure 3). The alignment of both point clouds was done on a stable part of the cliff, with a standard deviation of the error below 20 cm (Figure 3C). Not surprisingly, this one is less accurate than other studies using user-end camera and equivalent sensor to object distance (Eltner et al., 2016). In the collapsed area, the maximal horizontal distance between the two datasets is about 3.9 m. The collapsed volume (including a potentially hole between the cliff and the wall) was estimated to be about 225 m^3 using the point cloud comparison method described above. Based on Google Street images, we manually estimated the dimensions of this volume (15 m long x 10 m high x 1.5 m deep), getting a similar value.

The reasonably good results were due to the good image quality, the cliff proximity to the camera location, the good lighting, the absence of obstacles between the camera location and the wall, no vegetation and the efficient repartition of point of view

around the cliff (Figure 2A). "Basse Corniche" results (Figure 3 and Table 1) are the best results obtained among the three study areas.

4.2 Site 2 – Séchilienne Landslide

Eight point clouds of which seven of SfM-MVS process with GSV images were generated for "Séchillienne" landslide at six different time steps (from April 2010 to December 2016). Three different image sources were used: GSV print screens from Google Maps, GSV images saved from Google Earth Pro and images from a GoPro HERO4+ camera from a moving vehicle (Figure 4 and Table 1). Two different programs (VisualSFM and Agisoft PhotoScan) were used for image treatment. The number of 3D points on the landslide area varies from 9'500 to 25'000 points for a processing with VisualSFM, while 236'000 3D points were generated when using Agisoft PhotoScan. In comparison, 1'500'000 points were obtained on the same area using terrestrial photogrammetry with a 24 Mpx reflex camera. Results were aligned on a 50 cm resolution LiDAR scan of the landslide acquired in 2010. Then, the street view SfM-MVS point clouds were compared with a mesh from the LiDAR scan. Average distance of point clouds vary from -2.1 to 0.2 m (distance point to mesh in absolute values). The standard deviations vary from 1.4 m to 3.1 m (Figure 4 A-E and Table 1). SfM-MVS point clouds from Google Earth Pro images processed with Agisoft PhotoScan provide the best results (Figure 4G). These images have a resolution about 7.3 times higher than the print screens from Google Maps (1920x1200 pixels for GSV print screens from Google Maps versus 4800x3500 pixels for GSV images exported from Google Earth Pro).

Landslide changes between 2010 (LiDAR DEM) and 2015 (SfM-MVS) are observable with a material accumulation (red colour in Figure 4G) in the debris cone and some material losses in the upper part of the landslide (blue colour in Figure 4G). Unfortunately, the back in time function does not exist in Google Earth Pro and it is thus not possible to save old GSV images from Google Earth Pro. Finally, the comparison between the LiDAR mesh and the SfM-MVS cloud derived from GoPro HERO4+ camera images (Figure 4H) gives similar results to those obtained using the GSV images from Google Earth Pro (Figure 4G). Thus, the best results of the SVI-derived models were obtained with Agisoft PhotoScan when using Google Earth Pro images. Results were less accurate when using SfM-MVS processing with VisualSFM and lower resolution print screen images from Google Maps.

This case study shows a good correlation between our ground truth (i.e. LiDAR point cloud) and some SfM-MVS point clouds derived from SVI datasets. The adjustment between the LiDAR point cloud and SfM-MVS point clouds derived from SVI is a key factor defining the quality of the clouds comparison. This manual adjustment on stable areas was not easy to perform because of the low density of points on the SfM-MVS clouds derived from SVI. We noted a huge difference on the number of points between the different SfM-MVS clouds derived from SVI. This difference on the number of points shows the impacts of the image quality.

Images with low resolution and with low lighting generated a lower number of points compared to the models generated with the last generation of GSV cameras having higher resolution and more advanced sensors and pictures taken with favourable lighting conditions. The large distance between the road and the landslide considerably limits the final accuracy

due to low image resolution, as discussed in Eltner et al., 2015; the closest distance between the road and the centre of the landslide is 500 m and the largest distance between the upper part of the landslide and the point of view is about 1'400 m. Furthermore, the vegetation on the landslide foot and along the road as well as a power line partially obstruct the visibility of the study area. In addition, clouds are present on several images on the top of the scarp, degrading the upper part of the 3D point cloud. Results show that it is not possible to bring out changes in the landslide over the years because of the insufficient accuracy of the SfM-MVS point clouds with SVI, except for the 3D clouds resulting from the GSV images saved in Google Earth Pro and processed in Agisoft PhotoScan (Figure 4G). However, the main landslide structures such as little gullies observed in the failure zone and deposition area show an interesting approximation of the current landslide morphology as it was recorded with LiDAR.

4.3 Site 3 – Arly Gorges

Four point clouds of which three of SfM-MVS process derived from GSV images were generated on the "Arly gorges" site, at four different times (from March 2010 to December 2016). Three different images sources (GSV print screens from Google Maps, GSV images exported from Google Earth Pro and our own images acquired from a GoPro HERO5 Black) were used (Figure 5 and Table 1). Two different programs (VisualSFM and Agisoft PhotoScan) were tested. In addition, a LiDAR point cloud resulting from an assembly of six Optech Ilris scans has been used as ground truth.

The 3D point cloud from the GoPro Hero5 Black images has been roughly georeferenced thanks to the GNSS integrated in the camera; the three point clouds processed from GSV images and the LiDAR scan have been roughly aligned to this reference. Then the four SfM-MVS point clouds were precisely aligned on the LiDAR point cloud, which was considered as the reference cloud.

The analysis shows that the 2010 model derived from GSV images processed with VisualSFM gives the least accurate results (Figure 5A). We hardly perceive on that figure the wall of the tunnel entry and the wide cliff structures. The results of the point cloud from 2014 GSV images processed with the same program are slightly better (Figure 5B). The point cloud processed in Agisoft PhotoScan derived from 2016 GSV images saved from Google Earth Pro displays much better quality than the previous (Figure 5C). We now see the protective nets in the slope as well as the blue road sign announcing the tunnel. The vegetation is also observable.

The SfM-MVS point cloud derived from GoPro images taken standing along the road gives a significantly better representation of the scene (Figure 5D). Slope structures and protective nets are well modelled, but not the small vegetation. The comparison between the 2016 LiDAR scan (Figure 5E) and the three SfM-MVS with GSV images point clouds does not allow to identify terrain deformation on the cliff. Moreover, the source area of the rockfall is not observable from the GSV images because it is located higher in the slope, outside of the images.

A great majority of points consistently displayed distances between the LiDAR scan mesh and the SfM-MVS point clouds ranging between +/- 2 m (Figure 5E-5G). Protective nets degrade the results because it generates badly modelled surfaces

corresponding to the nets on some cliff sections (such as the red-blue section on the top-right of the July 2014 cloud (Figure 5F)).

A strong limiting factor on this site is the non-optimal camera locations. Indeed, the location of the cliff above a tunnel portal does not allow for a lateral movement between the camera positions with regard to the cliff. The maximal viewing angle (in blue colour on the Figure 2A) is about 35° compared to 170° for the site 1, and 115° for the site 2, that is 3 to 5 time smaller than for the other studied sites.

4.4 Discussion

The main limitation found in this study is that SfM-MVS processing is designed to retrieve the internal orientation of standard cameras, whereas the images used in this research do not correspond to a standard camera due the construction of the panoramas. Indeed, the main problem comes from the different deformations on GSV print screens or images due to the panoramas construction. Same strong radial deformations on each images, like on fisheyes images from GoPro cameras, can be processed without limitation with SfM softwares like Agisoft PhotoScan. In addition, images from GSV are often over- or underexposed (case study 3) and their resolution is low for distant subjects (cases study 2 and 3), making difficult to obtain good results with these constraints. Making zoomed print screens from GSV images do not allow increasing the SfM-MVS process results (case study 2) due to a low images resolution. Finally, the spatial repartition of SVI is often problematic because there are not enough images along the track path and because the road path does not often allow obtaining an efficient strategy concerning the camera positions around the studied area (case study 3). Accessing to RAW images together with valuable data of camera calibration would considerably help deriving 3D point clouds from GSV using modern photogrammetric workflows.

Our study highlighted important differences on 3D model reconstruction using different software, consistently with previous works (Micheletti et al., 2015; Gomez-Gutierrez et al., 2015, Niederheiser et al., 2016). Agisoft Photoscan performed better than VisualSFM when using both GSV images from Google Earth Pro (Figure 4F-G) and pictures acquired from a GoPro Hero camera (Figure 4H). Nevertheless, VisualSfM performed better than Agisoft Photoscan on print screens captures from SVI. The only difference between these sources of information is the resolution: 2.3 Mpx for print screens from Google Maps, 16.8 Mpx for images saved from Google Earth Pro and 12Mpx for GoPro camera, stressing the importance of picture resolution on the quality of the 3D model.

With the experience acquired during the research, we can highlight the following recommendations to improve results of SfM-MVS with SVI images. (A) Firstly, the distance between the image point of view and the subject and the size of the subject are important because it influences the pixel size on the subject. In study case 1, the location of the cliff next to the road (< 1 m) allows to get images with a good resolution for the studied object. In study case 2, the area under investigation is too far from the road (500 – 1'400 m) and small structures cannot be seen in the landslide. (B) Secondly, the ability to look at the scene from different angles (Figure 2A) is a determining factor to obtain good results. The greater is this "view angle", the better the results will be. Case study 1 with a view angle of almost 180° is optimal because the object is observable from

half a circle. View angle of case study 2 (115°) is enough to get many different views of the subject from different angles. The view angle is too narrow to have enough different point of view of the cliff on case study 3 (35°). (C) Thirdly, results are influenced by the image quality and especially by their exposition, contrast and type of sensor, which has progressively been improved during the last years. Image quality varies considerably on different images sets. Case study 1 is again the best study case in term of image quality. Both image sets have optimal solar exposition and shadows are not strong. Case study 2 has sets with very different images quality. Some sets are well exposed, others not. Clouds are present on few image sets. For case study 3, we have a lot of over- and underexposed images on behalf of the situation of the site (incised valley with a southwest oriented slope with a lot of light or shadow). The problem of images quality concerns Google too because it has removed from Google Maps very underexposed GSV images taken in August 2014 on site 3 at the end of 2016. With all these considerations and not surprisingly, the best SfM-MVS results were obtained with the case study 1, whereas the lower quality was obtained at study site 3.

According to the results, small-scale landslides and rockfalls (<1 m^3) can be detected when the slope or the cliff is close to the road (0-10 m), as it was shown on site 1. Conversely, large slope movements and collapses (>1'000 m^3) can be detected when the studied area is far away from the road (>250 m) like on site 2. The measured differences between the point clouds on stable areas show good results once the point clouds alignment is well done. Thus, we observed standard deviations of a decimetre on stable areas on site 1 (Figure 3C), between 0.5 and 1.1 m on site 2 and between 0.1 and 0.9 m on the tunnel entry on site 3. Standard deviations increase on site 2 and 3 when point clouds are compared on their entire surface (Figure 4 A2-H2, Figure 5 E-G and Table 1). This is attributable to the occurrence of slope movements generating material increase or decrease and thereby, increasing standard deviations of the error.

5 Conclusion

The proposed methodology provides interesting but challenging results due to some constraints linked to the SVI. The inconsistent image deformations and the impossibility of extracting the original images from a street view provider are the biggest limitations for 3D model reconstruction derived from SVI. The constraints (distance and obstacles between the studied area and the road, image quality, meteorological conditions, images repartition, number of images, shadows/highlighted areas) strongly limit the proposed approach.

However, SfM-MVS with SVI can be a useful tool in geosciences to detect and quantify slope movements and displacements at an early stage of the research by comparing datasets taken at different time series. This information is of great interest when no other data of the studied area has been obtained.

The quality of the final product was observed to be mainly dependent on the images quality and of the distance between the studied area and image perspectives. In this study it was possible to detect and characterize small-scale landslides and rockfalls (<1 m^3) for study areas relatively close to the road (from 0 to 10 m); complementarily, it was possible to detect large scale landslides or rock collapses (>1'000 m^3) over areas located far away from the road (hundred meters or more). In

other words, it will be difficult, if not impossible, to detect small-scale slope movements of a cliff or a landslide far away from the road with proposed approach.

A simple development to improve our proposed approach would be that Google add the back in time function into the Google Earth Pro software. In this case, it would be possible to save GSV images from any proposed time period and to process those images with Agisoft PhotoScan (Figure 4G) and thus to obtain better results than when using VisualSFM (Figure 4F). Knowing that Google services and functionalities of Google Maps and Google Earth are evolving over time, it is possible that SfM-MVS with GSV images will be more efficient and easier in a near future.

Despite of the observed limitations, the main interest of the proposed approach is the possibility to use archival imagery and deriving 3D point clouds of an area that has not been captured before the occurrence of a given event. This will allow increasing database on rock slope failures, especially for slope changes along roads which conditions are favourable for the proposed approach.

References

Abellan, A., Oppikofer, T., Jaboyedoff, M., Rosser, N.J., Lim, M. and Lato, M.J., 2014, Terrestrial laser scanning of rock slope instabilities. Earth Surface Processes and Landforms, v. 39, p.80-97.

Agisoft, L. L. C., 2015, Agisoft PhotoScan user manual, Professional edition, version 1.2.6.

Anguelov, D., Dulong, C., Filip, D., Frueh, Ch., Lafon, S., Lyon, R., Ogale, A., Vincent, L., Weaver, J., 2010, Google Street View: Capturing the world at street level. Computer, Vol. 43, IEEE, 32-38.

Carrivick, J. L., Smith, M. W., Quincey, D. J., 2016, Structure from Motion in the Geosciences. John Wiley & Sons.

Dubois, L., Chanut, M.-A., Duranthon, J.-P., 2014, Amélioration continue des dispositifs d'auscultation et de surveillance intégrés dans le suivi du versant instable des Ruines de Séchilienne. Géologues n°182, p50-55.

Durville, J.-L., Bonnard, C., Potherat, P., 2011, The Séchilienne (France) landslide: a non-typical progressive failure implying major risks, Journal of Mountain Science, Vol. 8, Issue 2, 117-123.

Eltner, A., Kaiser, A., Castillo, C., Rock, G., Neugirg, F. and Abellán, A., 2016, Image-based surface reconstruction in geomorphometry–merits, limits and developments. Earth Surface Dynamics, 4(2), pp.359-389.

Favalli, M., Fornaciai, A., Isola, I., Tarquini, S., Nannipieri, L., 2011, Multiview 3D reconstruction in geosciences, Computers & Sciences 44, 168-176.

Fey, C., Wichmann, V., 2016, Long-range terrestrial laser scanning for geomorphological change detection in alpine terrain – handling uncertainties. Earth Surf. Process. Landforms.

Fernández, T., Pérez, J. L., Cardenal, J., Gómez, J. M., Colomo, C., Delgado, J., 2016, Analysis of Landslide Evolution Affecting Olive Groves Using UAV and Photogrammetric Techniques. Remote Sensing, 8(10), 837.

Furukawa, Y., Ponce, J., 2010, Accurate, dense, and robust multiview stereopsis. Pattern Analysis and Machine Intelligence, IEEE Transactions on, 32(8), 1362-1376.

Furukawa, Y., Curless, B., Seitz, S. M., Szeliski, R., 2010, Towards internet-scale multi-view stereo. In Computer Vision and Pattern Recognition (CVPR), 2010 IEEE Conference on (pp. 1434-1441). IEEE.

France 3 : Important éboulement dans les gorges de l'Arly en Savoie, 2014, available at : http://france3-regions.francetvinfo.fr/alpes/savoie/important-eboulement-dans-les-gorges-de-l-arly-en-savoie-400849.html (last access 25 January 2017).

Géoportail, IGN (2016), 2016, available at http://www.geoportail.gouv.fr (last access 25 January 2017).

Girardeau-Montaut, D., 2011, CloudCompare-Open Source project. OpenSource Project.

Gómez-Gutiérrez, Á., de Sanjosé-Blasco, J.J., Lozano-Parra, J., Berenguer-Sempere, F. and de Matías-Bejarano, J., 2015, Does HDR pre-processing improve the accuracy of 3D models obtained by means of two conventional SfM-MVS software packages? The case of the Corral del Veleta Rock Glacier. Remote Sensing, 7(8), pp.10269-10294.

Google Street View, Understand Street View, 2017, available at https://www.google.com/maps/streetview/understand (last access 25 January 2017).

Google Maps, Google Inc. (2017), 2017, available at https://maps.google.com (last access 25 January 2017).

Google Earth Pro, version 7.1.2.241, Google Inc. (2013), 2013, available at https://www.earth.google.com/earth (last access 25 January 2017).

Guerin, A., Abellán, A., Matasci, B., Jaboyedoff, M., Derron, M.-H., Ravanel, L.: Brief communication: 3D reconstruction of a collapsed rock pillar from web-retrieved images and terrestrial LiDAR data – The 2005 event of the West face of the Drus (Mont-Blanc massif), Nat. Hazards Earth Syst. Sci. Discuss., doi:10.5194/nhess-2016-316, in review, 2016.

James, M. R., Robson, S., 2012, Straightforward reconstruction of 3D surfaces and topography with a camera, Accuracy and geosciences application, Journal of Geophysical research, Vol. 117, F03017.

Klingner, B., Martin, D., Roseborough, J., 2013, Street View Motion-from-Structure-from-Motion, Proceedings of the International Conference on Computer Vision, IEEE.

Kromer, R., Abellán, A., Hutchinson, J., Lato, M., Edwards, T., Jaboyedoff, M., 2015, A 4D Filtering and Calibration Technique for Small-Scale Point Cloud Change Detection with a Terrestrial Laser Scanner. Remote Sensing vol.7, pp.13029-13052; DOI: 10.3390/rs71013029.

Lichtenauer, J. F., Sirmacekb, B., 2015, A semi-automatic procedure for texturing of laser scanning point with google streetview images, The International Archives of the Photogrammetry, Remote Sensing and Spatial Information Sciences, Volume XL-3/W3, 109-114.

Le Roux, O., Schwartz, S., Gamond, J. F., Jongmans, D., Bourles, D., Braucher, R., Mahaney, W., Carcaillet, J., Leanni, L., 2009, CRE dating on the head scarp of a major landslide (Séchilienne, French Alps), age constraints on Holocene kinematics, Earth and Planetary Science Letters, Vol. 280, 236-245.

Lucieer, A., de Jong, S., Turner, D., 2013, Mapping landslide displacements using Structure from Motion (SfM) and image correlation of multi-temporal UAV photography, Progress in Physical Geography, Vol. 38(1), 97-116.

Luhmann, T., Robson, S., Kyle, S., Boehm, J., 2014, Close-range photogrammetry and 3D imaging. Walter de Gruyter.

Lowe, D., 1999, Object recognition from local scale-invariant features. International Conference of Computer Vision, Corfu Greece, 1150-1157.

Luhmann, T., Robson, S., Kyle, S., Boehm, J., 2014, Close-range photogrammetry and 3D imaging, Walter De Gruyter.

Micheletti, N., Chandler, J. H., Lane, S. N., 2015, Investigating the geomorphological potential of freely available and accessible Structure-from-Motion photogrammetry using a smartphone. Earth Surface Processes and Landforms, Vol 40(4), 473-486.

Nice-Matin : La basse corniche coupée en direction de Monaco après un éboulement, 2014, available at : http://www.nicematin.com/menton/la-basse-corniche-coupee-en-direction-de-monaco-apres-un-eboulement.1587292.html (last access 15 October 2015).

Niederheiser, R., Mokroš, M., Lange, J., Petschko, H., Prasicek, G., & Elberink, S. O., 2016, Deriving 3d Point Clouds from Terrestrial Photographs-Comparison of Different Sensors and Software. International Archives of the Photogrammetry, Remote Sensing and Spatial Information Sciences-ISPRS Archives, 41, 685-692.

Oppikofer, T., Jaboyedoff, M., Blikra, L., Derron, M.-H., Metzger, R., 2009, Characterization and monitoring of the Åknes rockslide using terrestrial laser scanning. Natural Hazards and Earth System Science 9: 1003–1019.

Rosser, N.J., Petley, D.N., Lim, M., Dunning, S.A., Allison, R.J., 2005, Terrestrial laser scanning for monitoring the process of hard rock coastal cliff erosion. Quarterly Journal of Engineering Geology and Hydrogeology 38(4): 363–375.

Royán, M.J., Abellán, A., Jaboyedoff, M., Vilaplana, J. M., Calvet, J.,2014, Spatio-temporal analysis of rockfall pre-failure deformation using Terrestrial LiDAR. Landslides, pp.1–13.

Ruggles, S., Clark, J., Franke, K. W., Wolfe, D., Reimschiissel, B., Martin, R. A., ... & Hedengren, J. D.,2016, Comparison of SfM computer vision point clouds of a landslide derived from multiple small UAV platforms and sensors to a TLS-based model. Journal of Unmanned Vehicle Systems, 4(4), 246-265.

Snavely, N., M. Seitz, S., Szeliski, R., 2006, Photo Tourism: Exploring Photo Collection in 3D. In SIGGRAPH 06, 835-846.

Snavely, N., 2008, Scene reconstruction and visualization from Internet photo collections, unpublished PhD thesis, University of Washington, USA.

Snavely, N., Seitz, S., Szeliski, R., 2008, Modeling the World from Internet Photo Collections Int J Comput Vision, Springer Netherlands, 80, 189-210

Streetside, Microsoft Inc. (2017), 2017, available at https://www.microsoft.com/maps/streetside.aspx (last access 25 January 2017).

Stumpf, A., Malet, J. P., Allemand, P., Pierrot-Deseilligny, M., Skupinski, G., 2015, Ground-based multi-view photogrammetry for the monitoring of landslide deformation and erosion. Geomorphology, 231, 130-145.

Tencent Maps, Tencent Inc. (2017), 2017, available at http://map.qq.com (last access 25 January 2017).

Turner, D., Lucieer, A., Watson, C., 2012, An Automated Technique for Generating Georectified Mosaics, from Ultra-High Resolution Unmanned Aerial Vehicle (UAV), Conference on 3D Imaging, Modeling, Processing, Visualization &

Transmission Imagery, Based on Structure from Motion (SfM) Point Clouds, Remote Sensing, 4(5), 1392-1410 IEEE,479-486.

Walstra, J., Chandler, J. H., Dixon, N., Dijkstra, T. A., 2007, Aerial photography and digital photogrammetry for landslide monitoring. Geological Society, London, Special Publications, 283(1), 53-63.

Wang, C.-P., Wilson, K., Snavely, N., 2013, Accurate Georegistration of Point Clouds Using Geographic Data, In 3D Vision – 3DV, IEEE, 33-40.

Westoby, M.J., Brassington, J., Glasser, N.F., Hambrey, M.J., Reynolds, J.M., 2012, 'Structure-from-Motion' photogrammetry: A low-cost, effective tool for geoscience applications, Geomorphology, Vol. 179, 300-314.

Wu, C., 2011, VisualSFM: A visual structure from motion system, available at http://ccwu.me/vsfm (last access 25 January 2017).

Zamir, A. R., Shah, M., 2010, Accurate Image Localization Based on Google Maps Street View, In Computer Vision – ECCV 2010, Springer, 255-268.

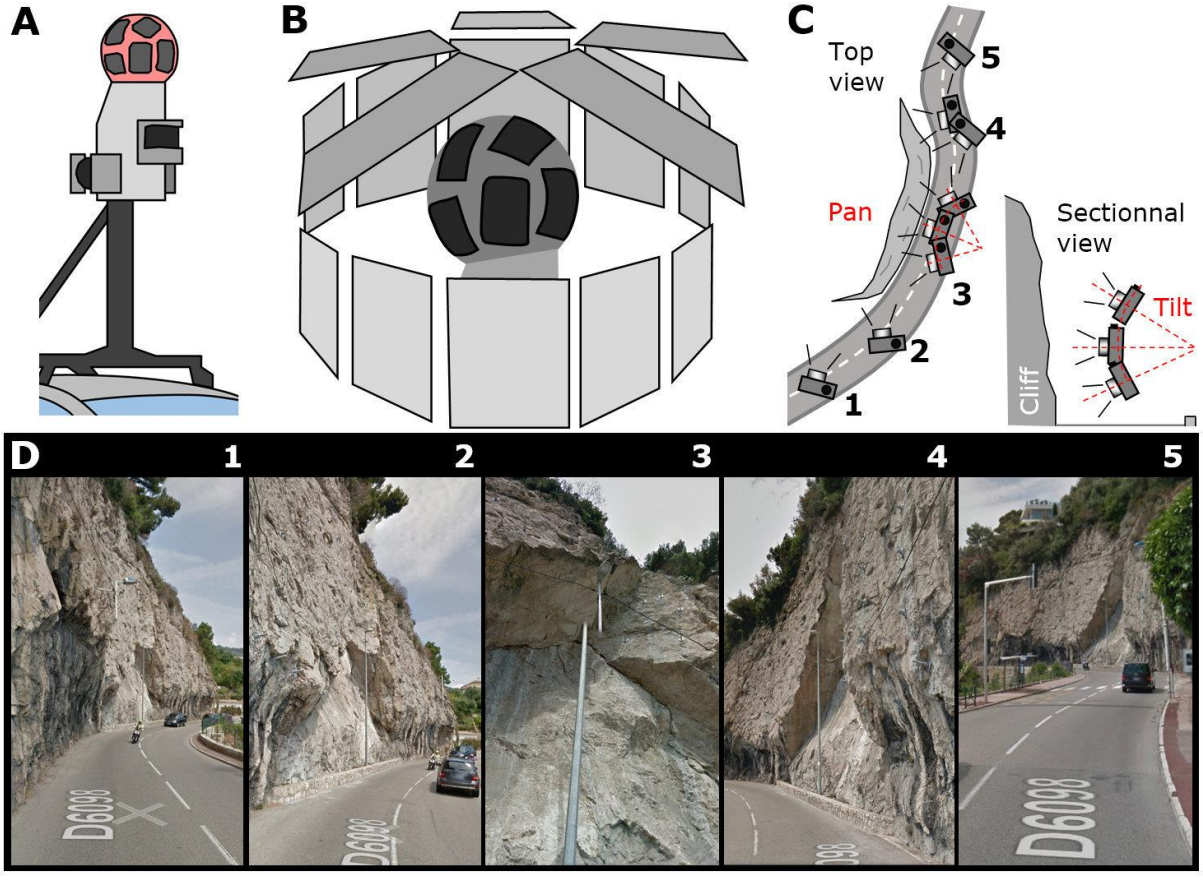

Figure 1: Google Street View (GSV) imagery functioning. A: Schema of the GSV spherical camera system mounted on a car roof. Sensors in black colour are LiDAR on which are draped the GSV images (based on Google Street View 2017). B: Functioning of the GSV spherical panorama built with fifteen images. C: Strategy of the GSV service for SfM-MVS photogrammetry. Numbers

Nat. Hazards Earth Syst. Sci. Discuss., doi:10.5194/nhess-2017-49, 2017
Manuscript under review for journal Nat. Hazards Earth Syst. Sci.
Discussion started: 9 February 2017

Natural Hazards and Earth System Sciences
Discussions

correspond schematically to the images in D. D: Screen captures of GSV photos from the study site 1. The image numbers correspond to those in C. Note the gap on the street-lamp in image 3 due to the panorama construction from the GSV pictures.

Figure 2: The three French studied sites (1: Basse-Corniche, 2: Séchilienne and 3: Arly gorges). A: Google Maps aerial view of the sites (red colour) with the road path (yellow colour) used to take the GSV images of the scenes and the view angle (blue colour) of the images point of view around the sites. B: First GSV of the sites. C: Last GSV of the sites.

Nat. Hazards Earth Syst. Sci. Discuss., doi:10.5194/nhess-2017-49, 2017
Manuscript under review for journal Nat. Hazards Earth Syst. Sci.
Discussion started: 9 February 2017

Natural Hazards and Earth System Sciences
Discussions

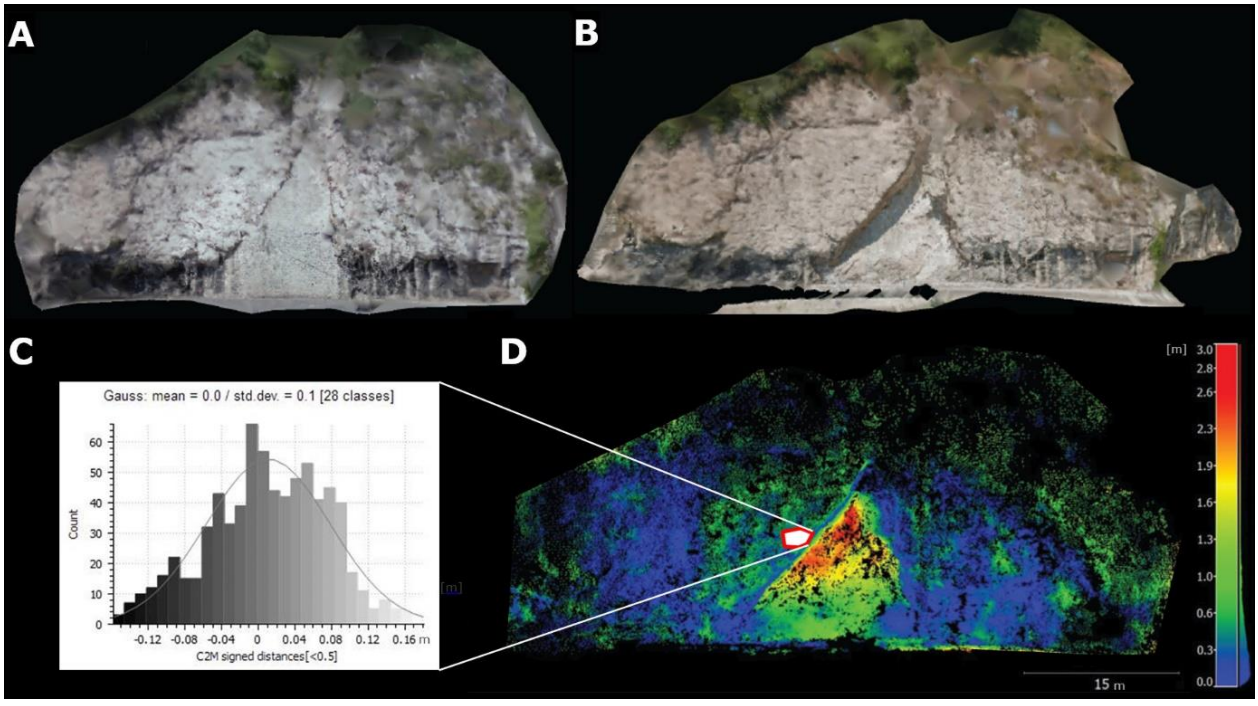

Figure 3: Results at site 1 "Basse-Corniche". A: 3D model produced with GSV images taken before the event in 2008. B: 3D model produced with GSV images taken after the event in 2014. C: Statistics on a small part of the wall (red colour polygon on figure D) of 7'510 points between the two point clouds. D: Comparison of the two point clouds of 2008 and 2014. The maximal horizontal depth of the cliff is about 3.9 m. The information on the pictures source and date and on the program used is given in Table 1.

Nat. Hazards Earth Syst. Sci. Discuss., doi:10.5194/nhess-2017-49, 2017
Manuscript under review for journal Nat. Hazards Earth Syst. Sci.
Discussion started: 9 February 2017

Natural Hazards and Earth System Sciences
Discussions

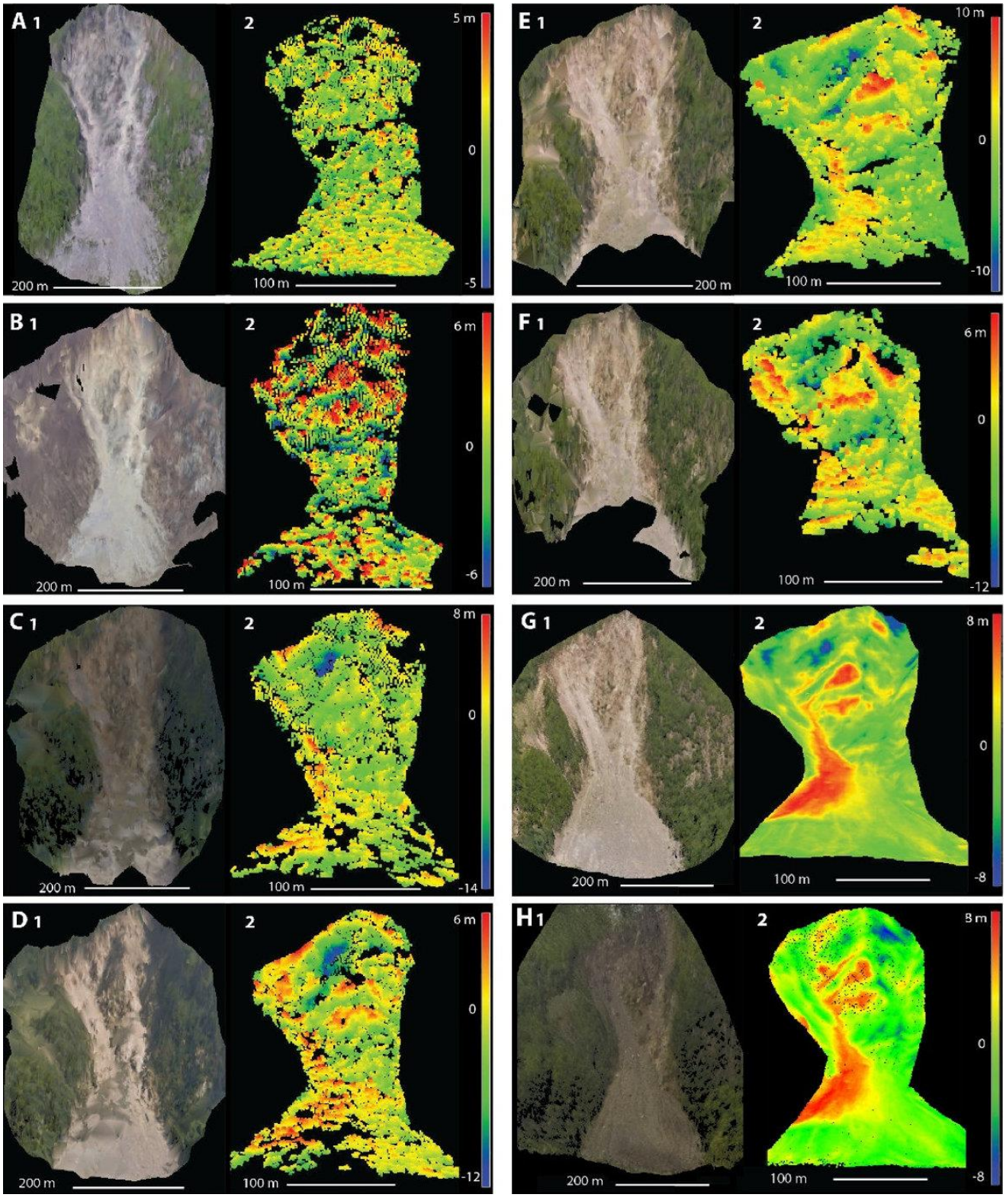

Nat. Hazards Earth Syst. Sci. Discuss., doi:10.5194/nhess-2017-49, 2017
Manuscript under review for journal Nat. Hazards Earth Syst. Sci.
Discussion started: 9 February 2017

Natural Hazards and Earth System Sciences
Discussions

Figure 4: Results at site 2 "Séchilienne". Eight points clouds from different images sets taken at six different time with three different image sources and processed with two different programs. Figures A1-H1: Meshs resulting from the respective point clouds. Figures A2-H2: point clouds comparison with a 50 cm LiDAR DEM from 2010 (red colour points is material increase; blue colour points are material decrease from the 2010 LiDAR cloud). The information on the pictures source and date and on the program used is given in Table 1.

Nat. Hazards Earth Syst. Sci. Discuss., doi:10.5194/nhess-2017-49, 2017
Manuscript under review for journal Nat. Hazards Earth Syst. Sci.
Discussion started: 9 February 2017

Natural Hazards and Earth System Sciences
Discussions
Open Access
EGU

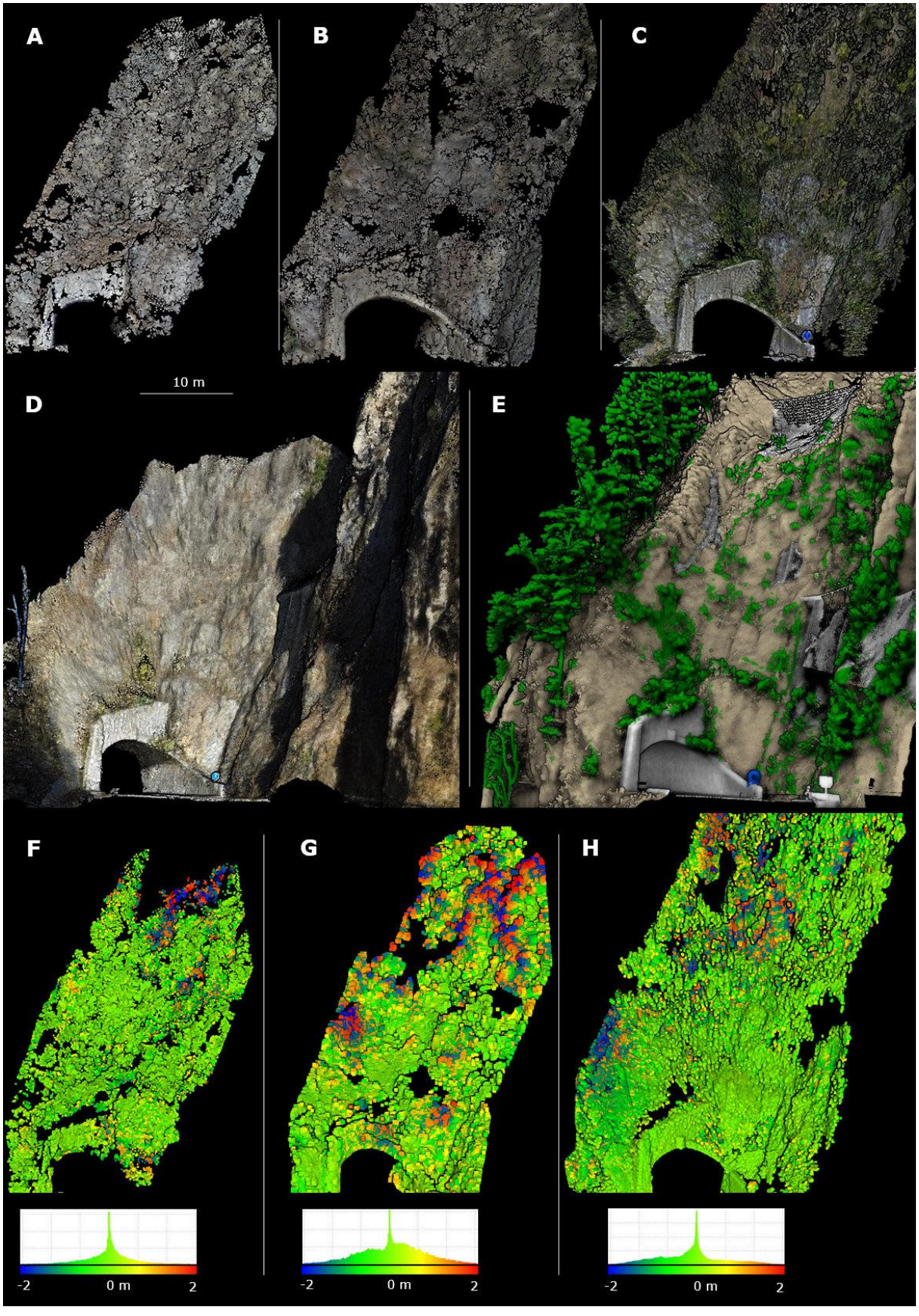

Nat. Hazards Earth Syst. Sci. Discuss., doi:10.5194/nhess-2017-49, 2017
Manuscript under review for journal Nat. Hazards Earth Syst. Sci.
Discussion started: 9 February 2017

Natural Hazards and Earth System Sciences
Discussions

Figure 5: Results at site 3 "Arly gorges". Five points clouds from four different images sets sources and processed with two different softwares and one LiDAR scan. A: March 2010 point cloud. B: July 2014 point cloud. C: August 2016 point cloud. D: December 2016 point cloud taken on foot with a GoPro camera. E: December 2016 LiDAR cloud from an assembly of six Optech terrestrial LiDAR scans. The grey colour elements in the cliff are the protective nets. F-G-H: March 2010, July 2014 and August 2016 point clouds compared with December 2016 LiDAR DEM (red colour points is material increase; blue colour points are material decrease from the 2016 LiDAR cloud). The information on the pictures source and date and on the program used is given in Table 1.

Table 1: List of the fourteen point clouds presented in this paper.

Site	Figure	Date	Images source	Images size [pixel]	Images number	Processing software	Number of points	Comparison				
								With	Min. [m]	Max. [m]	Average [m]	Std. dev. [m]
Site 1	Fig. 3A	2008.05	GSV, GM[1]	1920 x 1200	60	VisualSFM	150'000	2014.06[5]	-1.2	2.6	0.2	0.7
	Fig. 3B	2014.06	GSV, GM[1]	1920 x 1200	50	VisualSFM	182'000	2008.05[6]	-0.2	0.2	0	0.1
Site 2	Fig. 4A	2010.04	GSV, GM[1]	1920 x 1200	54	VisualSFM	18'000	LiDAR[7]	-5.5	4.9	-0.2	1.4
	Fig. 4B	2011.03	GSV, GM[1]	1920 x 1200	52	VisualSFM	9'500	LiDAR[7]	-6.6	6.8	-0.1	1.8
	Fig. 4C	2013.05	GSV, GM[1]	1920 x 1200	45	VisualSFM	12'500	LiDAR[7]	-13.9	7.9	-2.1	2.7
	Fig. 4D	2014.06	GSV, GM[1]	1920 x 1200	52	VisualSFM	25'000	LiDAR[7]	-12.8	6.3	-1.5	2.8
	Fig. 4E	2015.06	GSV, GM[1]	1920 x 1200	62	VisualSFM	23'500	LiDAR[7]	-11.4	9.7	-0.9	3.1
	Fig. 4F	2015.06	GSV, GEP[2]	4800 x 3500	80	VisualSFM	22'500	LiDAR[7]	-11.9	7.4	-1.7	3.1
	Fig. 4G	2015.06	GSV, GEP[2]	4800 x 3500	80	Agisoft PhotoScan	236'000	LiDAR[7]	-8.1	8.3	0.6	2.5
	Fig. 4H	2016.05	GoPro[3]	4000 x 3000	75	Agisoft PhotoScan	46'000	LiDAR[7]	-8.9	8.1	-0.2	2.7
Site 3	Fig. 5A, 5F	2010.03	GSV, GM[1]	1920 x 1200	66	VisualSFM	35'000	LiDAR[8]	-2.2	2.1	0.0	0.5
	Fig. 5B, 5G	2014.07	GSV, GM[1]	1920 x 1200	111	VisualSFM	53'000	LiDAR[8]	-2.2	2.3	0.1	0.7
	Fig. 5C, 5H	2016.08	GSV, GEP[2]	4800 x 3107	64	Agisoft PhotoScan	3'1850'000	LiDAR[8]	-2.3	2.5	-0.1	0.7
	Fig. 5D	2016.12	GoPro[4]	4000 x 3000	50	Agisoft PhotoScan	2'217'000	LiDAR[8]	-4.2	3.4	0	0.4